Oil-in-Water Zein Protein/Soybean Oil Microcapsules from Ultrasound-Assisted Emulsification: Stability, Morphology and Curcumin Inclusion/Release Studies

Alessandra Quarta , Chiara Del Balzo , Francesca Cavalieri , Raffaella Lettieri , Mariano Venanzi *

Posted Date: 10 October 2025

doi: 10.20944/preprints202510.0678.v1

Keywords: core-shell microcapsules; curcumin; protein microcapsule; ultrasound-assisted emul-sification; zein protein

 doi:10.20944/preprints202510.0678.v1

Article

Oil-in-Water Zein Protein/Soybean Oil Microcapsules from Ultrasound-Assisted Emulsification: Stability, Morphology and Curcumin Inclusion/Release Studies

Alessandra Quarta, Chiara Del Balzo, Francesca Cavalieri, Raffaella Lettieri and Mariano Venanzi *

Dept. of Chemical Science and Technologies, University of Rome Tor Vergata, via della Ricerca Scientifica 1, 00133, Rome, Italy

* Correspondence: venanzi@uniroma2.it

Abstract

Zein (ZP) is the major storage protein of corn (maize). It is safe, biodegradable, edible, and characterized by unique amphiphilic and self-assembly properties. These properties were exploited to prepare ZP/Soybean Oil (SO) filled microcapsules by ultrasound-assisted emulsification of oil in water (o/w) solutions under optimal experimental conditions. The morphology and stability of o/w ZP/SO microcapsules were characterized by optical spectroscopy (electronic circular dichroism, fluorescence), dynamic light scattering, and bright-field, laser confocal fluorescence and scanning electron microscopies. It is shown that ZP, due to its unique amphiphilic properties, forms a stable outer layer that protects the inner oily phase by diffusion of the confined compounds. Proof-of-principle studies on the inclusion and release of Curcumin, a very active anti-inflammatory and nutraceutical substance, from ZP/SO microcapsules under temperature and pH stimuli are also reported.

Keywords: core-shell microcapsules; curcumin; protein microcapsule; ultrasound-assisted emulsification; zein protein

1. Introduction

Encapsulation of active ingredients in microparticles is a green technology with a wide range of applications in food chemistry, cosmetics and theranostics [1]. Examples of microsystems able to entrap active materials, include polymeric nano- and microparticles, core–shell structures, microsponges and microspheres forming stable colloid emulsions in solution [2,3]. Among the others, ultrasound-assisted emulsification (UAE) is a simple, low-cost and effective method for preparing aqueous suspensions of microcapsules filled by oil-soluble active ingredients, *i.e.*, oil-in-water (o/w) microcapsules [4,5].

The microcapsule shell prevents the diffusion of confined compounds out of the inner phase, providing a barrier of nanometric thickness that can protect the embedded molecules from acidic, alkaline or enzymatic degradation. Moreover, polymeric capsules may respond to changes in pH, temperature or other external stimuli, so that they can release the entrapped materials under specific experimental conditions, thereby ensuring suitable targeting and programmed delivery of the encapsulated components [6]. Microcapsules made from proteins have the advantage of being intrinsically biocompatible and biodegradable and, for these properties, they have been extensively studied for pharmaceutical and food targeted applications [7,8].

 doi:10.20944/preprints202510.0678.v1

Zein protein (ZP), the primary storage protein in maize, is FDA-recognized as safe [9]. It is biodegradable, edible, and exhibits unique amphiphilic and self-assembly properties, with abundant availability from corn surpluses and bioethanol byproducts [10]. Applications of ZP include use in fibers, adhesives, coating, ceramics, inks, cosmetics, textiles, and biodegradable plastics [11–14]. Furthermore, ZP is known to form a robust, hydrophobic grease-proof coating that can be used as a biodegradable film and plastics, ensuring resistance against microbial attack [15,16]. However, ZP insolubility in water and its poor nutritional quality (negative nitrogen balance) limits its use in human food products, promoting, on the other hand, its industrial utilization in food packaging and coating [17].

From the molecular point of view, ZP is encoded in a large multigene family and is constituted by a heterogeneous mixture of polypeptides of different molecular size, solubility and charge [18]. Four main ZP fractions have been identified, *i.e.*, α- (19-22 kDa, 70-80%), β- (17 kDa, 10-20%), γ- (27 kDa) and δ- (10 kDa) ZP. Presently, more than 60 structures are deposited on the ZP UniProt KB database [19], and more than 40 for α-ZP [20]. The low ZP solubility in water and its prevalent hydrophobic character are primarily attributed to the high content of non-polar amino acids (more than 50%) in the protein's primary structure, and to the amidation as glutamines and asparagines of its glutamic residues (21-26%). However, ZP is soluble in binary solutions consisting of lower aliphatic alcohols and water, such as 50-90% aqueous ethanol [21]. It should be stressed that different ZP fractions show different solubility properties.

The secondary structure of ZP has been investigated by electronic circular dichroism (ECD) and FTIR spectroscopy. It is reported that ZP is characterized by a ~40-60% helical content, complemented by β-sheets (30%) and β-turns (20%) structures, [22–24] while there is no consensus on the tertiary structure of ZP. Argos et al. [25] proposed a ZP 3D model comprising nine adjacent, topologically anti-parallel helices, clustered by glutamine-rich "turns" or "loops". The polar and hydrophobic residues distributed along complementary helical surfaces developed intra- and intermolecular hydrogen bonding, so that ZP could be arranged in planes. It has also been shown that ZP is able to self-assemble into mesophases of different morphology depending on the specific experimental conditions [26,27]. In particular, ZP may lead to the formation of stable nanostructures, such as fibers, nanoparticles, microspheres and thin films, depending on the experimental conditions [28].

UAE is the most common technique used for the synthesis of oil-filled microcapsules and for the confinement of ingredients in the oily phase. The emulsification of oil is achieved by the shear stress produced by collapse of microbubbles under ultrasound pressure through multiple in-phase expansion and contraction steps [4]. Acoustic cavitation of bubbles boosts the disruption of oil droplets, facilitating the formation of stable emulsions [5].

Cavitation effects are highly dependent on the applied ultrasound frequency. The amount of energy released by the bubble collapse and the maximum bubble size before collapse (resonance size) are correlated, and inversely proportional to the applied frequency. Ultrasound parameters such as the frequency and the acoustic power can be tuned to control the number of cavitation events, the microcapsule size, and the surface roughness and structure [4].

Ultrasounds have already been used to prepare microcapsules stabilized by a protein network coating bubbles, droplets or other templates, which can be dispersed as an emulsion [29]. During the emulsification stage, bubbles or liquid droplets act as a 'template' for the protein shell, that forms a physical barrier at the interface between the inner oily phase and the aqueous solution. Reversible protein coating is achieved by exploiting hydrophobic effect and hydrogen bonding interactions, while irreversible coating takes place if covalent linkages, like disulfide bonds, are produced. In the latter case, the formation of covalent links can be facilitated by free radicals generated through high-frequency ultrasonic cavitation [4,5].

The amphiphilic character of ZP places the protein at the interface of the oil droplets dispersed in water, thus forming a tight and effective protective coating for the encapsulated compounds [30]. Although several studies focused on ZP/polymer or ZP/surfactant systems as stabilizers in emulsion

 doi:10.20944/preprints202510.0678.v1

formulations [31–34], relatively few efforts have been dedicated to the ultrasound-assisted production of pure ZP-coated microcapsules [30,35–38].

In this contribution, the stability and morphology of o/w ZP/soybean oil (SO) microcapsules, denoted in the following as ZP/SO MC, will be investigated by optical spectroscopy, dynamic light scattering and optical and electronic microscopy techniques. Furthermore, proof-of-principle experiments on the inclusion and release of Curcumin in/out of ZP/SO MC will be presented.

In particular, it was found that: i) MC number density and size were mainly determined by the ZP concentration in the emulsification solution, while ultrasound acoustic power and sonication time affected the MC structure and integrity over time; ii) the MC protein shell is stabilized by the formation of dityrosine linkages and the ZP secondary structure reorganization from α-helical to antiparallel β-sheet conformations, so that solubility of ZP/SO MC in 100% water can be achieved; iii) Curcumin was successfully loaded in ZP/SO MC and suitably released upon pH and temperature stimuli.

2. Results

2.1. Preparation of Oil-in-Water Zein/Soybean Oil Microcapsules by Ultrasound Assisted Emulsification

Details on the optimization of the experimental conditions for the preparation of ZP/SO MC by UAE are briefly reported in the Materials and Methods section (see below) and, more extensively, as Supplementary Materials (Section SM1). Very briefly, a set of experiments was designed to evaluate the microcapsules stability and size distributions by tuning several preparation parameters: acoustic power, sonication time, ZP and SO concentrations, storage conditions (Table SMT1, Figures SMF1-SMF6). Each system was monitored for a minimum of 5 days to a maximum of one month.

The optimal sonication conditions were therefore fixed as: 45 s sonication time, 20 kHz frequency, 220 W electric power. Under these experimental conditions, minimal oil/water phase separation was detected after 10 days. Stable ZP/SO MC were obtained only for ZP concentrations higher than 2 mg/mL. UAE of the formulation composed of 10 μL SO, 5 mg/mL ZP solutions in 1 mL EtOH/H_2O 70/30 (v/v) provided the best results in terms of stability and homogeneous size distribution of ZP/SO MC (Figures SMF1-SMF4).

The formation of ZP/SO MC could be clearly detected by optical microscopy imaging, right after the ultrasound treatment (Figure 1A) and up to 4 days of storage at room temperature (Figure 1D). Figure 1D, where a crown of small nanocapsules decorating the border of larger ZP/SO MC can be observed, clearly reveals the occurrence of a time-dependent coalescence process that strongly depended on the ZP and SO concentrations. Optical microscopy images of ZP/SO MC produced by UAE of solutions of different ZP concentrations (5, 7.5 and 10 mg/mL) and SO amounts (10, 25 and 50 μL) are reported as SM (Figure SMF5). It was found that the MC number density and stability are both highly dependent on the ZP/SO concentration ratio.

 doi:10.20944/preprints202510.0678.v1

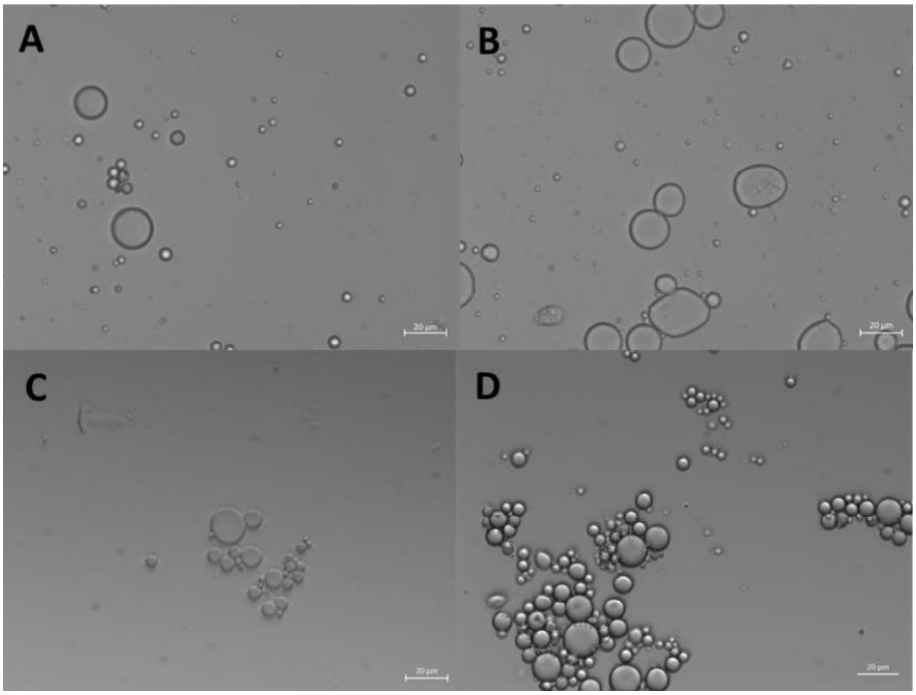

Figure 1. Optical microscopy images of o/w emulsions from 1 mL EtOH/H_2O 70/30 (v/v) ZP solution and 50 µL soybean oil. A: 2.5 mg/mL ZP, t=0; B: 5 mg/mL ZP, t=0; C: 2.5 mg/mL ZP, t = 4 days; D: 5 mg/mL ZP, t = 4 days. Scale bar: 20 µm.

For comparison, o/w emulsions were also formed by UAE of EtOH/H_2O 70/30 (v/v) and SO solutions under the same sonication conditions. In this case, a rapid phase separation between the oil and the aqueous solvent was observed. On the contrary, ZP/SO MC showed, at longer times, the formation of a precipitate that can be easily redissolved in an aqueous solution by gently shaking the test tube.

Interestingly, dried ZP/SO MC can be successfully redispersed in 100% water, maintaining the same morphology, structure and size distribution (Figure SMF6), even after 25 days from re-dissolution. This is a crucial result, in view of real applications of ZP-coated MC. The reasons for the exceptional stability of ZP/SO MC in pure water, despite the poor solubilty of ZP in aqueous solutions, are under current investigation.

2.2. Morphological Characterization of o/w ZP/SO Microcapsules

The globular morphology of ZP/SO MC is clearly shown by the bright-field optical microscopy image (63x) reported in Figure 2. The dark border of the microcapsules is attributed to the ZP shell, positioned at the o/w interface, while SO mainly composes the more transparent inner phase.

 doi:10.20944/preprints202510.0678.v1

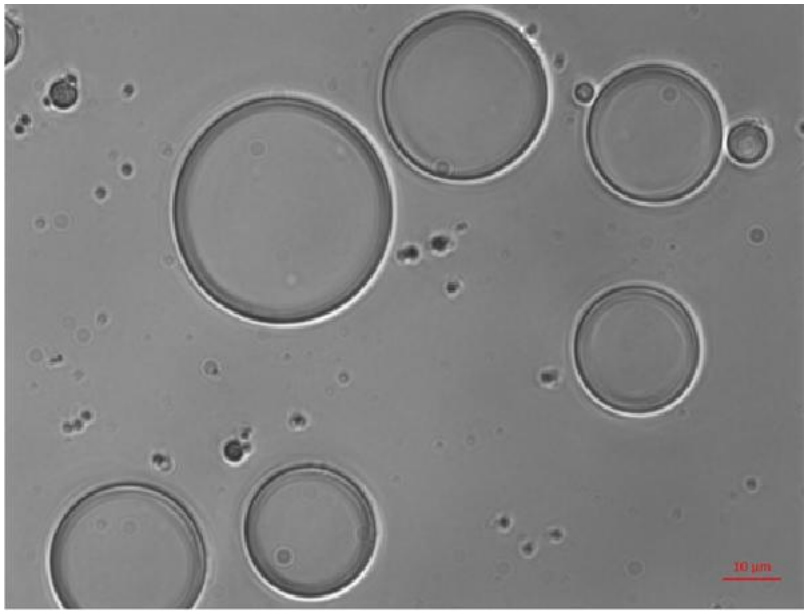

Figure 2. Bright-field optical microscopy image (63x) of o/w ZP/SO microcapsules prepared by UAE of 1 mL 5.0 mg/mL ZP EtOH/H_2O 70/30 (v/v) and 10 µL soybean oil solution. Sonication conditions: frequency =20 kHz; power= 220W; continuous mode. Scale bar: 10 µm.

The stability and morphology of ZP/SO MC were closely monitored for 5 days. It was found that the microcaspules, produced under optimal experimental conditions, remained in a metastable state for several days (Figures SMF1-SMF3), despite the insurgence of a time-dependent coalescence process. This phenomenon is clearly visible in the bright-field optical microscopy images of ZP/SO MC reported in Figure 3, taken after 4 days since preparation.

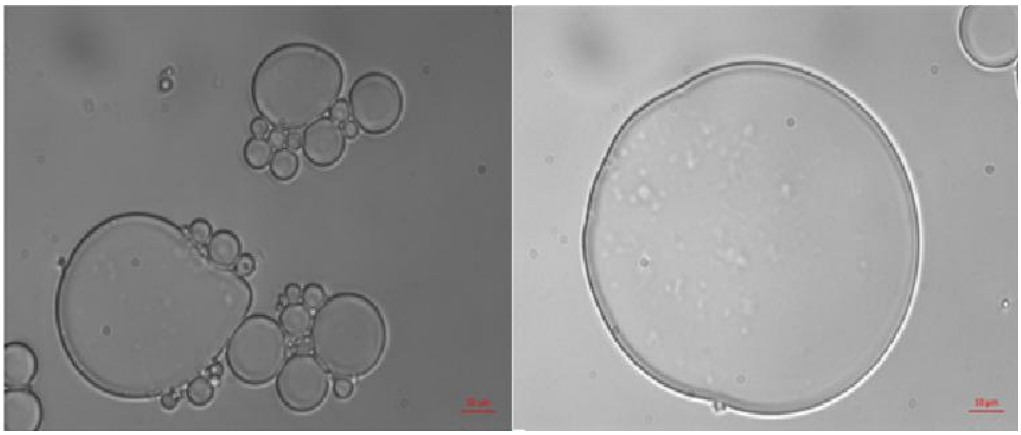

Figure 3. Bright-field (microscopy image (63x) of o/w ZP/SO microcapsules after 4 days since UAE of 1 mL 5.0 mg/mL ZP EtOH/H_2O 70/30 (v/v) solution and 10 µL soybean oil. Sonication conditions: frequency =20 kHz; power= 220W; continuous mode. Scale bar: 10 µm.

Interestingly, in the larger microcapsules imaged in Figure 3, nanometric ZP coacervates can be easily recognized in the inner oily phase. Analysis of the size of ZP/SO MC provides average diameters comprised in the 9-17 µm range, altough microcapsules featuring diameters of about 100 µm could also be imaged.

Nile Red (NR), a well-known solvatochromic dye, was included in the oily phase of o/w ZP/SO MC to monitor the oil partition in the microcapsules prepared by UAE. NR is an excellent dye for the detection of intracellular lipid droplets by fluorescence microscopy, because its fluorescence is almost completely quenched in water, while it is strongly enhanced in a hydrophobic environment [39].

 doi:10.20944/preprints202510.0678.v1

Recently, Weissmueller et al. successfully encapsulated NR in the hydrophobic environment of ZP nanocarriers, obtained by flash nanoprecipitation [13].

NR-labelled ZP/SO MC were therefore observed by optical microscopy, collecting both bright-field and fluorescence images. The microstructures revealed by the two imaging techniques strongly overlapped, indicating that the ZP/SO MC are filled by SO/NR oil (Figure SMF7). Clustered ZP/SP/NR MC produced by coalescence (Figure SMF8), are clearly visible after 3-4 days from the UAE preparation, suggesting that the formation of large microcapsules proceed through the merging of ZP outer layers and the pooling of the oil content.

To get further evidence on their core-shell morphology, ZP/SO MC were also stained with Rhodamine B (RhB). It is well known that RhB can be easily conjugated to ZP, exploiting electrostatic, hydrogen bonds and van der Waals interactions [40].

ZP/SO MC embedding NR in the SO inner phase (Figure 4A) or stained with RhB (Figure 4B) were therefore imaged by Confocal Laser Scanning Fluorescence Microscopy (CLSFM). Besides the confirmation of the NR localization in the inner oily phase, clear evidence of the ZP(RhB) crown shell at the o/w interface can be observed in the RhB stained microstructures (Figure 4B), despite the faint background noise due to residual RhB in solution. The complementarity of the red fluorescence emission signals in NR and RhB stained samples can be easily appreciated from Figures 4A and 4B. A distinct demarcation line exists between the clustered particles when the oil is stained by NR, and the net border line denoting the ZP(RhB) fluorescent crown. These results prove the ZP/SO MC microstructure composed of a SO-filled core and a ZP outer shell.

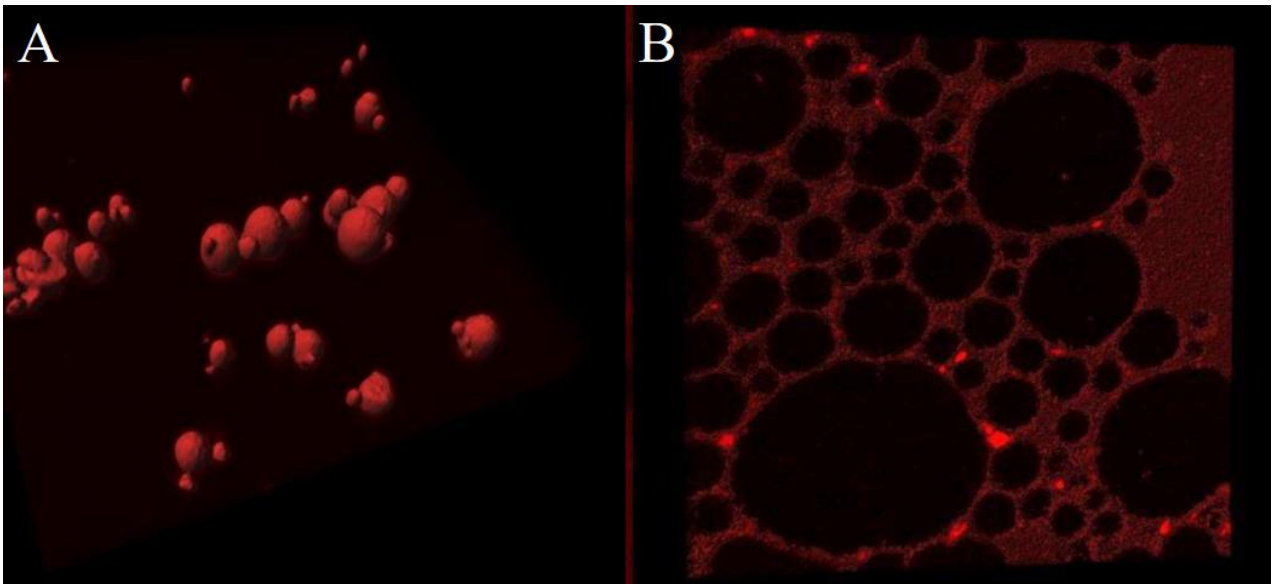

Figure 4. 3D fluorescence confocal microscopy image of o/w ZP/SO microcapsules from 10 mg/mL ZP EtOH/H_2O 70/30 (v/v) and 10 µL Soybean oil solution. A: Nile Red was added to SO before the synthesis. B: Rhodamine B was added to the ZP solution before the synthesis. Sample volume: 1 mL; sonication conditions: power= 220 W; time = 45 s, frequency = 20 kHz; continuous mode; test tube in ice bath. Scale bar: 10 µm.

Field Effect Environmental Scanning Electron Microscopy (FE-ESEM) experiments [41,42] were also carried out comparing freshly synthesized ZP/SO MC with the same sample after 18 days of storage at room temperature (Figure 5). The FE-ESEM image of an EtOH/H_2O 70/30 (v/v)/SO emulsion (control sample) is also reported as SM (Figure SMF9) for comparison. Contrary to what observed in Figure SMF9, where microstructures of any morphology could be detected, many ZP/SO microstructures were imaged by FE-ESEM (Figure 5), evidencing once more the role of the ZP shell in the stabilization of the oil droplets. However, freshly synthesized ZP/SO MC show remarkable morphological differences with respect to 18 days-old samples. In particular, the 18-days-old protein microstructures gave rise to rather elongated droplets, denoting degradation of the protein shell integrity and SO leakage (note the different scale of Figures 5A and 5B).

 doi:10.20944/preprints202510.0678.v1

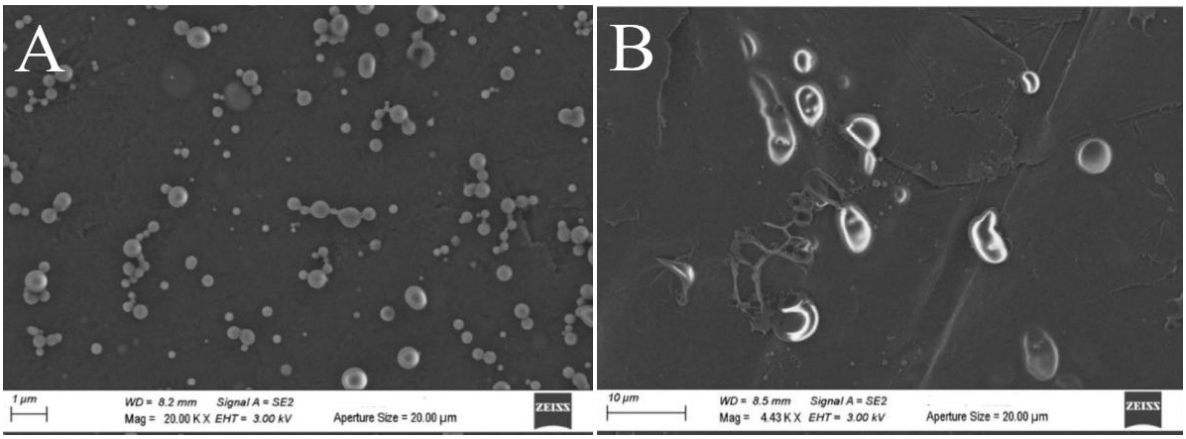

Figure 5. FE-ESEM images of o/w ZP/SO emulsions from 10 mg/mL Zein EtOH/H_2O 70/30 (v/v) and 10 µL soybean oil solutions. A: day of synthesis. Scale bar: 1 µm. B: after 18 days. Scale bar: 10 µm. Sonication parameters: power= 220 W; time= 25 s; frequency=20 kHz; continuous mode.

2.3. Optical Spectroscopy Studies of ZP/SO Microcapsules

UV absorption, fluorescence emission and ECD studies were performed to get an insight into the secondary structure of ZP deposited at the o/w interface of ZP/SO MC. We found that ZP dissolved in 70/30 (v/v) ethanol/H_2O solution shows two absorption bands in the near UV wavelength region peaked at 280 nm and 320 nm, that can be assigned to the Tyr [43] and dityrosine chromophores, respectively [44] (Figure SMF10). Dityrosine is a natural component of ZP, produced by environmental stress and protein modification [45], and it has been detected and quantified in previous studies [46].

ZP fluorescence emission spectra obtained by excitation at λ_{ex}=283 nm and λ_{ex}=315 nm are reported in Figure SMF11, where an emission maximum at λ_{em}=310 nm, typical of the tyrosine monomer, and a long-wavelength broad emission extending from 340 to 540 nm, and ascribable to dityrosine groups can be observed, respectively [43]. Interestingly, the fluorescence emission spectrum of ZP in ZP/SO MC (Figure 6) shows a substantial quenching of the Tyr monomer emission, and a relatively larger contribution of the dityrosine emission. This finding suggests that Tyr-Tyr interactions and the formation of dityrosine crosslinks may contribute to stabilize the protein shell of ZP/SO MC.

 doi:10.20944/preprints202510.0678.v1

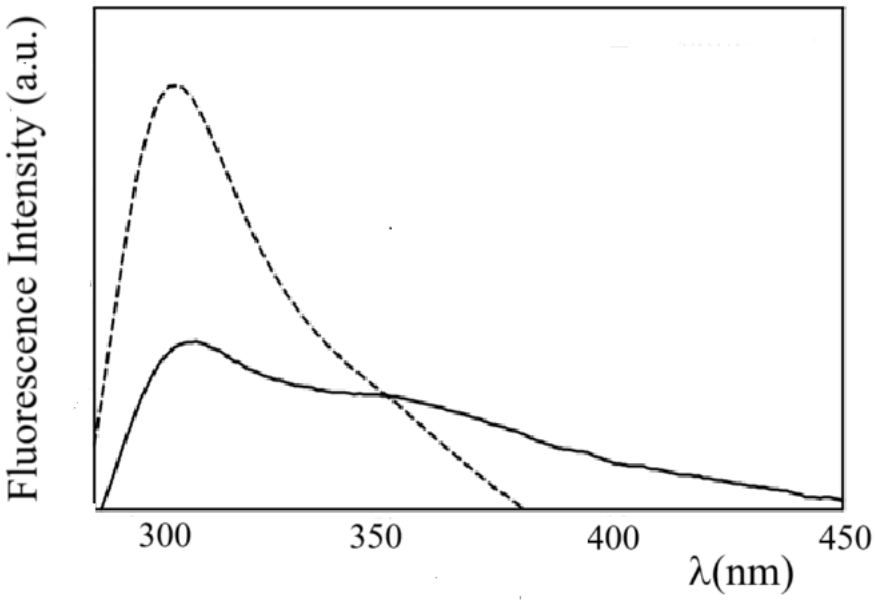

Figure 6. Fluorescence emission spectra of Zein protein in EtOH/H_2O 70/30 (v/v) (dashed line) and ZP/SO microcapsules (continuous line) (λ_{ex}=278 nm).

Important insights on the structural modification of ZP involved in the formation of the protein shell of ZP/SO MC are provided by ECD experiments. The ECD curves reported in Figure 7, clearly show that, while ZP in EtOH/H_2O 70/30 v/v solution predominantly attains a helical conformation, ZP in ZP/SO MC undergoes a conformational transition, principally populating β-sheet secondary structures. This finding, together with the fluorescence evidence reported above, suggests that the protein shell in the ZP/SO MC is further stabilized by layering interactions between the ZP building blocks attaining a β-sheet conformation. This conclusion is supported by the deconvolution of ECD curves carried out through BestSel code (Table 1) [47], that confirms that a conformational transition from helical to β-sheet structures takes place when ZP in solution is involved in the formation of ZP/SO MC.

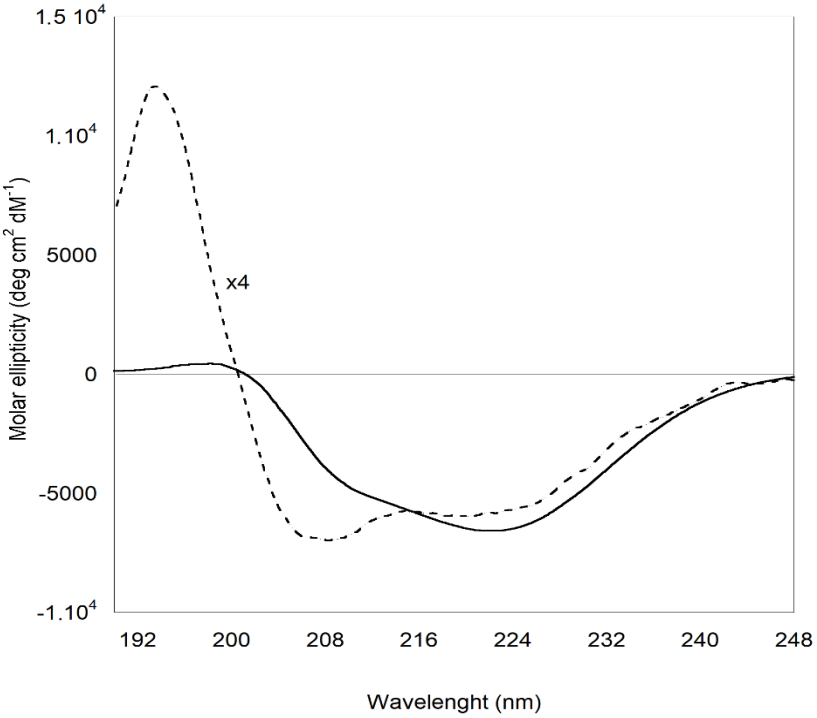

 doi:10.20944/preprints202510.0678.v1

Figure 7. Electronic Circular Dichroism spectra of Zein protein in EtOH/H_2O 70/30 (v/v) (dotted line) and ZP/SO microcapsules (continuous line). The CD profile of ZP was magnified by a factor 4 for clarity.

Table 1. Secondary structure of ZP in solution and in ZP/SO microcapsules from ECD experiments (T=25°C).

ZP (ZP/SO microcapsules) (%)	ZP (70/30 v/v EtOH/H_2O) (%)	Secondary structure
14.3	48.6	α-helix
42.4	6.1	antiparallel β-sheet
13.8	13.9	β turns
29.6	31.3	others

2.4. Stability of ZP/SO Microcapsules Under Temperature and pH Stimuli

The stability of ZP/SO MC in the 25°-70°C temperature range and 2-11 pH interval was investigated by Rayleigh Light Scattering (RLS) and Dynamic Light Scattering (DLS) experiments. As can be observed in Figure SMF12, the light scattering intensity of ZP/SO MC solutions (RLS measurements) showed a continuous decrease in the temperature range comprised between 30°C and 70°C, that could be associated to a drop in the particle number density and dimensions. DLS measurements also revealed that the average hydrodynamic radius of ZP/SO MC strongly decreases with the temperature, varying from 2.0 ± 0.2 μm at 25°C to 200 nm at 70°C (Figure SMF13).

It was found that thermal bursting preferentially occurs for microcapsules characterized by a particle size larger than a 'critical dimension', and that resistance to temperature breaking increased as the microcapsule size decreased, following an exponential trend similar to those reported in Figures SMF12 and SMF13 [48]. Those results can be therefore explained in terms of a progressive breaking of ZP/SO MC of larger dimensions as the temperature increases, allowing for the survival of microcapsules of nanometric dimensions.

A ZP/SO MC size reduction was also observed by RLS measurements at pH 2, while at pH higher than 7.3 (isoelectric point), the microcapsule average size notably increased, most likely due to coalescence of the formed microcapsules (data not shown).

Interestingly, size distribution analysis of DLS experiments at different pH's (Figure SMF14) show a single size distribution at pH 7.3 (isoelectric point) and at pH 5.5 (preparation condition), while at acid (pH 4.0 and pH 1.9) and alkaline (pH=8.3 and pH=11.2) pH's, two and three size distributions were obtained by deconvolution of the DLS data, indicating the heterogeneous character of the system at those extreme pH values.

Zeta potential (ζ) measurements revealed that, at pH 5.5 (preparation condition), ζ=+35.4 mV, a clear indication of the stability of ZP/SO MC under these experimental conditions. In this case, repulsive interactions between the charged interfaces inhibited the growth of microcapsules by coalescence. Interestingly, at the isoelectric point (pH=7.3), the zeta potential markedly decreased (ζ=+18.6 mV), suggesting that at this pH, coalescence phenomena could be favored.

2.5. Encapsulation and Release of Curcumin into/from ZP/SO Microcapsules

Curcumin [bis(4-hydroxy-3-methoxyphenyl)-1,6-heptadiene-3,5-dione] is a natural yellow-orange dye derived from the rhizome of *Curcuma Longa*, a member of the ginger family Zingiberaceae. It shows unique pharmaceutical and nutraceutical properties, due to its antioxidant, antibacterial and anti-inflammatory activities, as well as recognized safety [49].

Besides its important bioactive properties, Curcumin was chosen for inclusion studies because it lacks solubility in water, it is soluble in oil up to 2.90 ± 0.15 mg per oil gram [50], and it is strongly fluorescent [51]. These properties make Curcumin a proper candidate for its successful encapsulation in o/w microcapsules, and a suitable probe for fluorescence imaging. The inclusion of Curcumin in

 doi:10.20944/preprints202510.0678.v1

ZP nanoparticles and ZP-polymer hybrid assemblies has already been studied for delivery of food ingredients or therapeutics [52–61].

The UV-Vis absorption, fluorescence emission and excitation spectra of Curcumin in SO and ethanol are reported in Figures SMF15 and SMF16, respectively. As can be seen in the reported figures, the absorption and fluorescence spectra of Curcumin in SO are more structured with respect to the absorption and emission spectra in ethanol. In particular, the fluorescence emission peak of Curcumin is shifted from 486 nm in SO to 530 nm in ethanol, as a consequence of spectral relaxation in a polar solvent [62].

Curcumin has therefore been used as a probe to test the ability of ZP/SO MC to encapsulate an active ingredient using UAE. Bright field optical and fluorescence microscopy measurements revealed that Curcumin was successfully encapsulated into the ZP/SO MC oily phase, as shown in Figure 8. It should be noted that in Figure 8, the Curcumin fluorescence signal is overlapped to the ZP/SO microcapsules imaged by bright field optical microscopy, confirming the successful inclusion of Curcumin in the inner oily phase of ZP/SO MC.

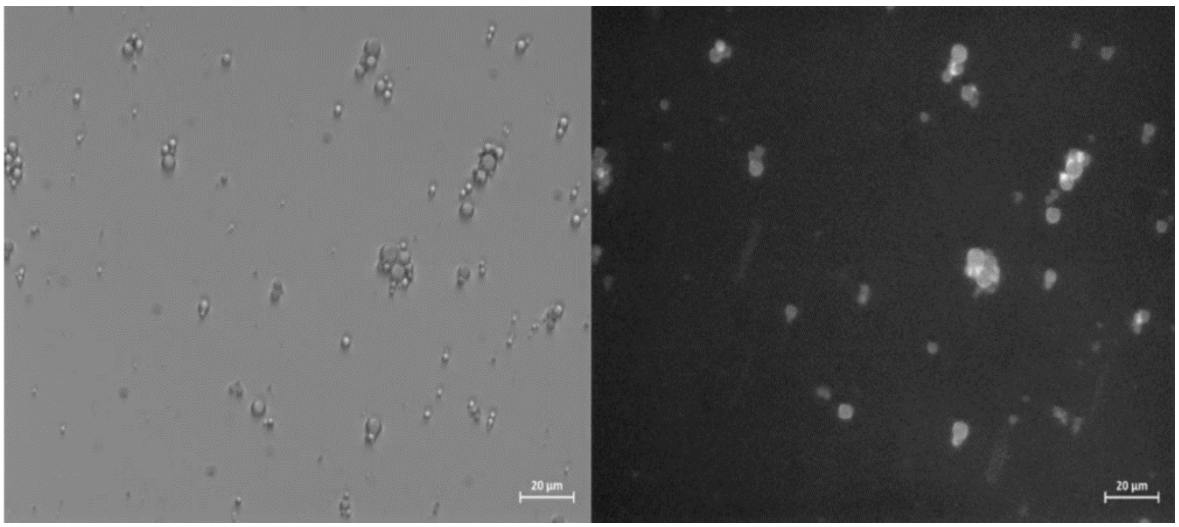

Figure 8. Bright field optical (left) and fluorescence (right) microscopy images of ZP/SO microcapsule encapsulating Curcumin. Curcumin has been included in soybean oil prior to the synthesis. Scale bar: 20 µm.

Noteworthy, the fluorescence emission spectrum of Curcumin in ZP/SO MC ($\lambda_{em,max}$=498 nm) occurs in a wavelength region intermediate between that one of its fluorescence emission spectrum in SO ($\lambda_{em,max}$=486 nm), and those in EtOH and EtOH/H_2O 70/30 ($\lambda_{em,max}$=530 nm), as shown in Figure SMF17. This result indicates that Curcumin is encapsulated in the oily phase of ZP/SO MC, but it is experiencing a more polar environment [62]. This finding suggests a preferential location of Curcumin near the ZP shell, coating the microcapsules, or in ZP coacervates. This hypothesis is supported by the results of Hu *et al*. that synthesized core-shell ZP nanoparticles coated by a Pectin hydrophilic outer layer fortified in the hydrophobic inner phase by Curcumin. Interestingly, Curcumin was found to interact preferentially with ZP through its aromatic groups and inter-ring chains [52].

CLSFM imaging of ZP/SO/Curcumin MC were obtained measuring the Curcumin fluorescence emission when excited at λ_{ex}= 418 nm. Figure 9 clearly shows that the Curcumin is embedded into the microcapsule inner phase and that the microcapsules maintain their globular morphology upon the Curcumin inclusion. Interestingly, CLSFM also shows low fluorescent Curcumin coacervates in water solution and in the inner core of ZP/SO MC, imaged as nanometric white spots.

 doi:10.20944/preprints202510.0678.v1

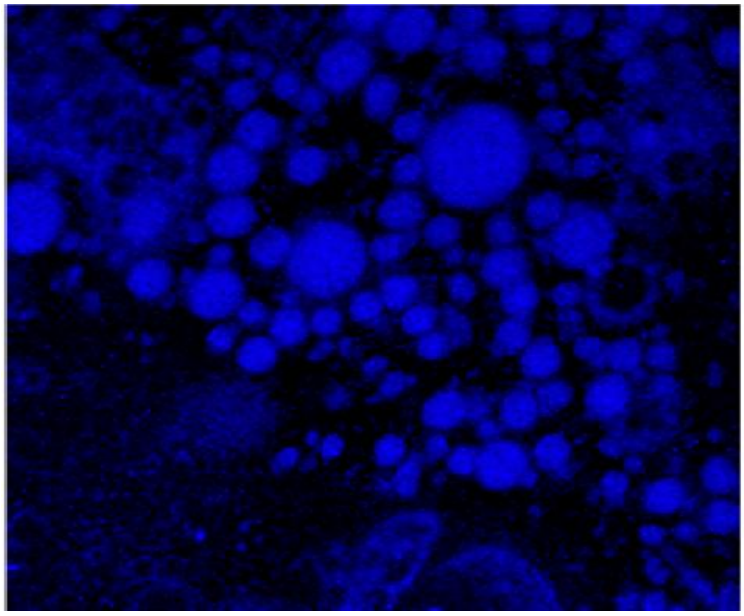

Figure 9. Confocal Laser Scanning Fluorescence Microscopy imaging of ZP/SO/Curcumin microcapsules. It can be noted the presence of low fluorescent ZP/Curcumin coacervates in aqueous solution and embedded in the inner oily phase of ZP/SO microcapsules.

This finding allowed us to use the very different fluorescence quantum yield of Curcumin in SO and in EtOH/H_2O to monitor the Curcumin release form ZP/SO MC upon pH and temperature stimuli.

Interestingly, varying the pH from pH=5.5 to pH 1.7, a marked decrease of the Curcumin fluorescence intensity could be observed (Figure SMF18). This finding indicates that the critical pH for the Curcumin release is around pH=4, as also suggested by pH-dependent DLS experiments (Figure SMF14).

Temperature-dependent RLS and DLS experiments have already assessed that a significant reduction in the number density and size of ZP/SO MC can be detected between 30° and 40°C (Figures SMF12 and SMF13, respectively).

Therefore, to get information on the mechanism of the Curcumin release from ZP/SO/Curcumin MC, we analyzed the time dependence of the Curcumin fluorescence intensity in this temperature range, where the perturbation of the ZP/SO MC system is maximum. In particular, kinetic experiments carried out at T=32, 35, 37 and 40°C on ZP/SO/Curcumin MC (pH 5.3) have shown a biexponential decrease of the Curcumin fluorescence intensity (Figure 10).

 doi:10.20944/preprints202510.0678.v1

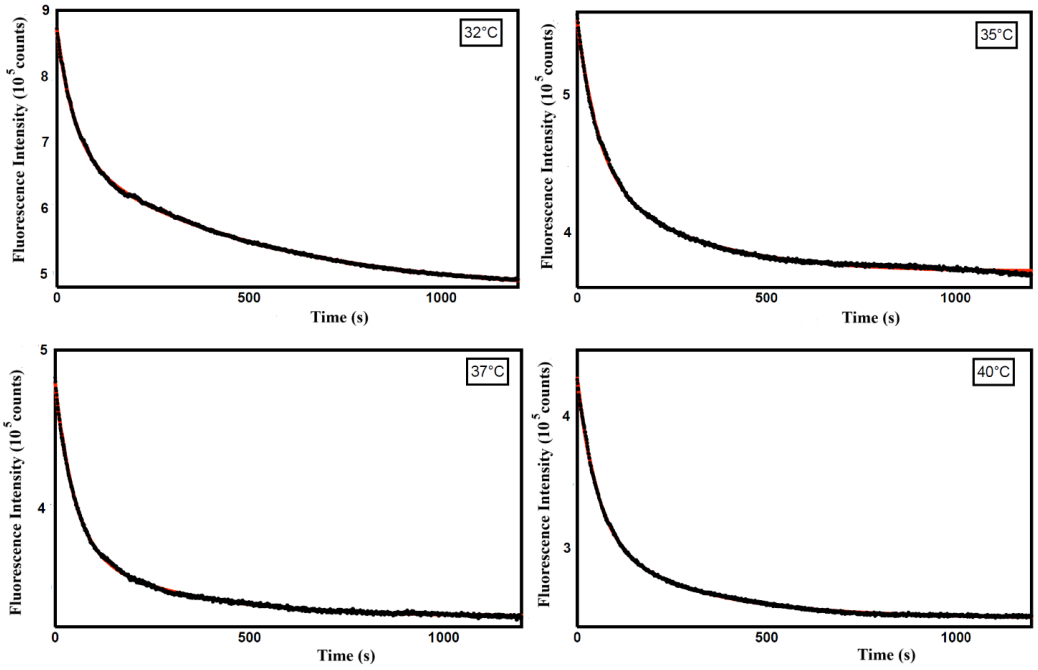

Figure 10. Fluorescence emission intensity as a function of time (seconds) of Curcumin in ZP/SO/Curcumin microcapsules at different temperatures (32°C, 35°C, 37°C, 40°C). Black line: experimental data; red line: bi-exponential fitting curve.

The rate constants, obtained from a bi-exponential fitting of the Curcumin fluorescence emission intensity with time through the equation

$$F(t)= \alpha_1 \exp(-k_1 t) + \alpha_2 \exp(-k_2 t)$$

are reported in Table 2.

Table 2. Kinetic rate constants (k_i) and weights (a_i) obtained from a bi-exponential fitting of the time-dependent Curcumin fluorescence emission intensity at different temperatures (pH 5.3).

$k_2(10^{-3}\ s^{-1})$	(a_2)	$k_1(10^{-2}\ s^{-1})$	(a_1)	Temperature (°C)
2.00 ± 0.02	(0.53)	2.14 ± 0.02	(0.47)	32
3.8 ± 0.1	(0.42)	1.81 ± 0.05	(0.58)	35
3.53 ± 0.08	(0.31)	1.88 ± 0.03	(0.69)	37
3.66 ± 0.05	(0.36)	1.93 ± 0.02	(0.64)	40

These results indicate that Curcumin release from ZP/SO MC follows a complex mechanism, characterized by, at least, two diffusion coefficients. This effect is most likely related to the heterogeneous distribution of Curcumin within the ZP/SO MC environment. So, on the basis of the a_1 and a_2 values at the different temperatures, we are tempted to assign the faster rate constant to Curcumin molecules positioned at the interface of the protein shell or within the ZP coacervates imaged by CLSFM experiments and the slower rate constant to Curcumin molecules located in the inner oily phase of ZP/SP MC. A comprehensive understanding of this issue clearly deserves further investigation.

3. Materials and Methods

3.1. Materials

3.1.1. Products

ZP sample was supplied by Sigma Aldrich [maize z1C2(541924, UniProt access numbers Q41896 and P04700] as dry powder and used as such without further purification or pre-treatment.

 doi:10.20944/preprints202510.0678.v1

According to the product information, the sample consists of two αZP of 22 and 24 KDa, characterized by a 66% and 63% helical conformation, respectively. ZP was solubilized in EtOH/H_2O 70/30 (v/v) under stirring. All the solutions for spectroscopy and microscopy experiments were freshly prepared from this same batch, and sealed in a dry, cool, and dark environment.

Curcumin (powder, min. 95% p/p) was purchased from Galeano srl (Italy), and used as such without further purification. SO, NR, RhB were purchased by Sigma Aldrich. Spectroscopic absolute ethanol (anhydrous, ≥ 99.9 %) was purchased from Carlo Erba. Milli-Q filtered water was obtained from a Millipore system (18.2 MΩ cm) at 25°C.

3.1.2. Preparation of o/w ZP/SO Microcapsules

Optimal experimental conditions for the preparation of o/w ZP/SO MC by UAE were established carrying out several experiments at different ZP concentrations (5, 7.5, 10 mg/mL), Soybean oil volumes (10, 20, 50 μL), ultrasound applied powers (110, 165, 220 W), sonication times (25, 30, 45 s) (Table SMT1). In a typical experiment, 10 μL SO were added to 5 to 10 mg ZP dissolved in 1 mL EtOH/H_2O 70/30 (v/v), and a 3 mm diameter ultrasound horn (Branson Digital Sonifier) was placed at the o/w interface. Sonication was carried out at 20 kHz frequency for 25 s at 220 W acoustic power. To reduce the temperature shock at the o/w interface induced by sonication, the system was immersed in an ice bath during the process. The obtained microcapsules were stored in a test tube at room temperature. Long-time storage of ZP/SO MC was carried out at 4°C, in a dry environment, and in the dark.

3.1.3. Inclusion/Release of Dyes and Active Compounds in ZP/SO Microcapsules

NR was included into ZP/SO microcapsules, by using SO stained with NR during the microcapsule preparation. The stained SO was stored under dark conditions at 4 °C. NR UV-Vis absorption and fluorescence spectra in SO are peaked at λ_{max}=510 nm and λ_{max}=570 nm, respectively.

ZP/SO MC were also stained by dissolving RhB in ZP EtOH/H_2O 70/30 (v/v), following the standard conditions for microcapsule preparation. RhB UV-Vis absorption and fluorescence spectra are located in the 500-580 nm and 550-680 nm wavelength region, respectively.

Curcumin (bis(4-hydroxy-3-methoxyphenyl)-1,6-heptadiene-3,5-dione) was added to SO and dissolved under stirring, storing the Curcumin/SO solution under dark conditions at 4 °C. Curcumin/SO was included in ZP/SO MC under standard operative conditions for microcapsule preparation. The release of Curcumin from ZP/SO MC under temperature and pH stimuli was monitored measuring the decreasing Curcumin fluorescence emission intensity when the drug, embedded into the SO inner phase, enters the aqueous phase.

3.2. Methods and instrumentation

3.2.1. UV–Vis Absorption Spectroscopy

UV-Vis absorption experiments were carried out with a Cary 100 Scan spectrophotometer (Varian, Middelburg, Netherlands) equipped with a Peltier thermostat (JASCO EHCS-760), using quartz cuvettes (Hellma Analytics) with optical lengths of 1 and 0.5 cm.

3.2.2. Electronic Circular Dichroism (ECD)

ECD experiments were carried out using a Jasco J-1500 CD spectropolarimeter (Jasco International Co.) using a cell holder equipped with a Peltier thermostat (PTC-510). The setup was purged with ultra-pure nitrogen gas. Spectra were recorded in the far-UV wavelength range, i.e., from 190 to 250 nm (amide region), and from 250 to 350 nm for the aromatic region (tyrosine), using a scan speed of 20 nm/min, a bandwidth of 2 nm, and a sensitivity of 20 mdeg. For each sample, the spectra were accumulated 10 times to maximize the signal-to-noise ratio. The solvent spectrum was subtracted for background correction. Quartz cuvettes (Hellma) with optical lengths of 1 mm were

 doi:10.20944/preprints202510.0678.v1

used. Data analysis for secondary structure determination was performed relying on the BestSel code [47].

3.2.3. Steady-State Fluorescence

Steady-state fluorescence experiments were carried out using a Fluoromax-4 spectrofluorometer (Horiba, Jobin Yvon) equipped with automatically controlled Glan-Thomson polarizers and single photon counting (SPC) detection. The temperature was set through an external thermostat Julabo F25, allowing for a maximum oscillation of ±0.1°C. Emission and excitation spectra were acquired using a 1 cm quartz cell (Hellma) and 3/3 nm excitation (ex) and emission (em) slits opening. 4/10 mm asymmetric quartz cell (Hellma), 1/1 nm ex/em slits were used for Curcumin in SO, while a 5 mm quartz cell (Hellma) and 1.5/1.5 nm ex/em slits were used for spectral measurements of Curcumin embedded in ZP/SO microcapsules. For this experiment, a cut-off emission filter was used to minimize light scattering contamination. Unless otherwise stated, fluorescence intensities are reported as signal-to-reference [count per second (cps)/microamperes (μA)] units. All the measurements were carried with optical densities lower than 0.1 at the excitation wavelength to minimize inner filter effects (IFE). IFE correction was applied to all the measured fluorescence spectra [63].

3.2.4. Optical Microscopy

Widefield microscopy images were obtained with a Zeiss microscope, Axio Scope A1 (Carl Zeiss, Oberkochen, Germany) equipped by a Mercury Lamp HBO 50 and CCD AxioCam ICm1 (Zeiss). The images were acquired with the software Zen-Blue (Zeiss) using magnification air (10x, 20x, 40x, 63x) and oil immersion (100x) objectives. Fluorescence imaging was performed in single channel mode of excitation (red channel for NR and RhB, blue channel for Curcumin). Images and particles diameters were analyzed using the software ImageJ [64].

Confocal Laser Scanning Fluorescence Microscopy experiments were carried out using an Olympus IX-81 inverted microscope coupled to a confocal scanning equipment FV1000 (Olympus, Shinjuku, Tokyo, Japan). Laser excitation was achieved at λ_{exc}=495 and 514 nm. Images were captured with a 40x oil immersion objective adding 4x and 5x zoom (160-200x total magnification). 3D image reconstruction was developed using commercial software.

3.2.5. Field Emission-Environmental Scanning Electron Microscope (FE-ESEM)

ZP/SO MC were imaged by a FE-ESEM LEO 1530 (Zeiss) microscope. Measurements were carried out placing a 5 μl ZP/SO MC solution on a graphite substrate, vacuum-packed for 30 minutes before recording topography information [65].

3.2.6. Light Scattering Experiments

Rayleigh Light Scattering (RLS) intensities of ZP/SO MC solutions were measured using the same fluorescence equipment described above, reporting the RLS intensities as signal-to-reference [count per second (cps)/microamperes (μA)]. Both excitation and emission monochromators were set at λ_{ex}=λ_{em}=600 nm, well outside the sample absorption or fluorescence emission regions. 5x5 mm quartz cells (Hellma) were used, with 0.5/0.5 nm ex/em slits opening.

Dynamic Light Scattering (DLS) experiments were carried out using a DLS Zetasizer Nano ZS (ZEN0040, Malvern Instruments, Malvern, IK) equipped with a He-Ne laser. ζ-potential measurements were carried out using the same equipment, equipped with appropriate cells. All the experiments were carried out in triplicate.

4. Conclusions

In this work, ZP/SO MC were prepared by UAE under optimal experimental conditions, producing SO oil droplets coated by a protein shell as the result of the emulsification process, and

 doi:10.20944/preprints202510.0678.v1

the unique ZP amphiphilic properties. It has been shown that the size distribution and number density of ZP/SO MC can be controlled by the combined effects of the applied ultrasound acoustic power, sonication time, ZP/SO concentration ratio and temperature. In particular, the ZP concentration turned out to be the most influential parameter, as regards the particle number density and size, while the applied acoustic power and sonication time mainly affect the microcapsule structure and integrity over time. This is because the acoustic power is related to shear forces, that are fundamental in the assembly of the protein units at the interface of the oil droplets [2]. Combining all the available information, optimal experimental conditions for preparing stable o/w ZP/SO MC were determined as: 1/20 oil/[EtOH/H_2O 70/30 (v/v)] ratio, 10 mg/mL ZP concentration, 10 μL SO, 20 kHz sonication frequency, 220 W acoustic power, 25 s sonication time in an ice bath. Under these experimental conditions, ZP/SO MC with average diameters of 0.9 ± 0.3 μm, showing slow MC coalescence and particle number density drop over 5 days, were obtained.

The ZP/SO MC morphology was characterized by optical microscopy, CLSFM and FE-ESEM imaging, providing direct evidence of the structure of protein microcapsules, *i.e.*, a SO inner phase stabilized by a ZP outer shell coating. Noteworthy, the oil core is preserved when coalescence occurs, resulting in larger oil-filled microcapsules. It was observed that the ZP-coated microcapsules grew until a critical size was achieved followed by collapse and rupture of the protein microcapsules. Dispersibility and stability in water of dried ZP/SO MC have also been investigated, finding that, although ZP is not soluble in water, ZP/SO MC can be successfully transferred and stored in aqueous solutions, with a water content as high as H_2O/EtOH 90/10 (v/v) and even 100% H_2O, a crucial result in view of future applications.

Fluorescence spectroscopy experiments have shown that ZP/SO MC are stabilized by the formation of tyrosine-tyrosine cross-linking and interprotein stacking interactions. CD data supported this scenario, as they displayed a protein structural reorganization from α-helical to antiparallel β-sheet structures.

The stability of ZP/SO MC in the 20-70°C temperature range and 2-11 pH interval were investigated by DLS experiments. It was found that the size of the protein microcapsules decreased almost continuously for increasing temperatures and at lower pH's, while at alkaline pH's coalescence of the microcapsules followed by their rupture and formation of micrometric oil droplets was observed.

Finally, as a proof-of-principle experiment, the ability of ZP/SO MC to encapsulate Curcumin, a fluorescent molecule showing unique pharmaceutical and nutraceutical properties, was tested and confirmed by optical microscopy and LCSFM imaging. The release of Curcumin from ZP/SO MC upon pH and temperature stimuli was also investigated, monitoring the decrease of the Curcumin fluorescence intensity upon diffusion from the microcapsule inner oily phase to the aqueous environment. Kinetic experiments in the critical temperature region comprised between 32 and 40°C revealed the complex character of the Curcumin diffusion pathways, most likely associated to the heterogeneous distribution of Curcumin molecules in the ZP/SO microcapsules.

It should be noted that the utilization of Curcumin in food and supplement products is still limited because of its extremely low (3×10^{-8} M) water solubility, poor chemical stability, and low oral bioavailability. These drawbacks make Curcumin difficult to incorporate into many products and to be solubilized in the aqueous fluids within the gastrointestinal tract. Moreover, a major factor that limits Curcumin bioavailability is its rapid degradation by hydrolysis and chemical instability under physiological conditions. Encapsulation seems to be the method of choice to enhance Curcumin solubility, stability and bioavailability [52–58,66].

The UAE encapsulation protocol proved to be successful, and Curcumin was efficiently included and retained into the ZP/SO MC here investigated. These results set a promising ground for future studies on the subject, considering the existing barriers to ZP transfer and delivery, passing through the stomach and the gastrointestinal tract [67,68]. I*n vivo* studies concerning the capacity of ZP microcapsules to preserve the encapsulated Curcumin, and allowing for its controlled release in applicative environments will be the object of future studies.

Supplementary Materials. The following supporting information can be downloaded at the website of this paper posted on Preprints.org. **SM1:** Set-up of experimental conditions for o/w ZP/SO MC preparation (Table SMT1, Figures SMF1-SMF6,). SM2: Morphological characterization of o/w ZP/SO MC (Figures SMF7-SMF9). SM3: Spectroscopic characterization of ZP/SO MC (Figures SMF10,SMF11). SM4: Stability of ZP/SO microcapsules under pH and Temperature stimuli (Figures SMF12-SMF14); SM5: Spectroscopy characterization of Curcumin in solution and in ZP/SO MC (Figures SMF15-SMF18).

Author's contribution: Conceptualization, F.C., M.V.; Methodology: A.Q., F.C.; Formal analysis: F.C., M.V.; investigation, A.Q., C.D,B, R.L.; resources: F.C., M.V.; data curation: A.Q., C.D.B., R.L.; writing-original draft preparation: M.V.; writing—review and editing, F.C., R.L.; supervision, M.V.; funding acquisition, F.C.

Funding: This project received funding from the European Union Horizon 2020 Research and Innovation Program under the Marie Skłodowska-Curie grant agreement no. 872233 (''PEPSA-MATE'').

Data Availability Statement: The data presented in this study are available on request from the corresponding author.

Acknowledgments: Dr. Antonio Rinaldi is gratefully acknowledged for having made possible FE-ESEM measurements at ENEA-Casaccia (Rome, Italy).

Conflicts of Interest: The authors declare no conflict of interest.

References

1. Bah, M.G.; Bilal, H.M.; Wang, J. Fabrication and application of complex microcapsules: A review. *Soft Matter* **2020**, *16*, 570-590. https://doi.org/10.1039/C9SM01634A
2. Ariaudo, D.; Cavalieri, F.; Rinaldi, A.; Aguilera, A.; Lopez, M.; Perez, H.G.; Felipe, A.; del Carmen Dominguez, M.; Ruiz, O.; Martinez, G.; Venanzi, M. Alginate Microsponges as a Scaffold for Delivery of a Therapeutic Peptide against Rheumatoid Arthritis. *Nanomaterials* **2023**, *13*, 2709. https://doi.org/10.3390/nano13192709
3. Lengyel, M.; Kállai-Szabó, N.; Antal, V.; Laki, A.J.; Antal, I. Microparticles, microspheres, and microcapsules for advanced drug delivery. *Scientia Pharmaceutica* **2019**, *87*, 1-10. https://doi.org/10.3390/scipharm87030020
4. Leong, T.S.H.; Martin, G.J.O.; Ashokkumar M. Ultrasonic encapsulation – A review. *Ultrason. Sonochem.* **2017**, *35*, 605–614. https://doi.org/10.1016/j.ultsonch.2016.03.017
5. Taha A.; Emam, A.; Ismaiel, A.; Ashokkumar, M.; Xu, X.; Pan, S.; Hu, H. Ultrasonic emulsification: An overview on the preparation of different emulsifiers-stabilized emulsions. *Trends Food Sci. Technol.* **2020**, *105*, 363–377. https://doi.org/10.1016/j.tifs.2020.09.024
6. Tortora, M.; Cavalieri, F.; Mosesso, P.; Ciaffardini, F.; Melone, F.; Crestini, C. Ultrasound driven assembly of lignin into microcapsules for storage and delivery of hydrophobic molecules, *Biomacromolecules* **2014**, *15*, 1634–1643. https://doi.org/10.1021/bm500015j
7. Ramos, R.; Bernard, J.; Ganachaud, F.; Miserez, A. Protein-based encapsulation strategies: Toward micro- and nanoscale carriers with increased functionality. *Small Sci.* **2022**, *2*, 2100095. https://doi.org/10.1002/smsc.202100095
8. Dissanayake, T.; Bandara, N. Protein-based encapsulation systems for co-delivery of bioactive compounds: Recent studies and potential applications. *Curr. Opin. Food Sci.* **2024**, *57*, 101181. https://doi.org/10.1016/j.cofs.2024.101181
9. Lawton, J.W. Zein: A history of processing and use. *Cereal Chem.* **2002**, *79*, 1–18. https://doi.org/10.1094/CCHEM.2002.79.1.1
10. Shukla, R.; Cheryan, M. Zein: The industrial protein from corn. *Industrial Crops and Products* **2001**, *13*, 171-192. https://doi.org/10.1016/S0926-6690(00)00064-97
11. Irache, J.M.; González-Navarro, C.J. Zein nanoparticles as vehicles for oral delivery purposes. *Nanomed.* **2017**, *12*, 1209–1211. https://doi.org/10.2217/nnm-2017-0075.
12. Girija Aswathy, R.; Sivakumar, B.; Brahatheeswarani, D.; Fukuda, T.; Yoshida, Y.; Maekawa, T.; Sakthi Kumar, D. Biocompatible fluorescent Zein nanoparticles for simultaneous bioimaging and drug delivery application. *Adv. Nat. Sci. Nanosci. Nanotechnol.* **2012**, *3*, 025006. https://doi.org/10.1088/2043-6262/3/2/025006.103

 doi:10.20944/preprints202510.0678.v1

13. Weissmueller, N. T.; Lu, H. D.; Hurley, A.; Prud'homme, R. K. Nanocarriers from GRAS Zein proteins to encapsulate hydrophobic actives. *Biomacromolecules* **2016**, *17*, 3828–3837. https://doi.org/10.1021/acs.biomac.6b01440.
14. Hurtado-López, P.; Murdan, S. Zein microspheres as drug/antigen carriers: A study of their degradation and erosion in the presence and absence of enzymes. *J. Microencapsul.* **2006**, *23*, 303–314. https://doi.org/10.1080/02652040500444149.
15. Beck, M.I.; Tomka, I.; Waysek, E. Physico-chemical characterization of Zein as a film coating polymer: A direct comparison with ethyl cellulose. *Int. J. Pharm.* **1996**, *141*, 137–150. https://doi.org/10.1016/0378-5173(96)04630-3.
16. Wang, Q.; Xian, W.; Li, S.; Liu, C.; Padua, G.W. Topography and biocompatibility of patterned hydrophobic/hydrophilic Zein layers. *Acta Biomater.* **2008**, *4*, 844–851. https://doi.org/10.1016/j.actbio.2008.01.017.104
17. Sharif, N.; Fabra, M.J.; López-Rubio, A. Nanostructures of Zein for encapsulation of food ingredients, in Biopolymer Nanostructures for Food Encapsulation Purposes, Elsevier, 2019, 217–245. https://doi.org/10.1016/B978-0-12- 815663-6.00009-4.
18. Song, R.; Llaca, V.; Linton, E.; Messing, J. Sequence, regulation, and evolution of the maize 22-kD α-Zein gene family. *Genome Res.* **2001**, *11*, 1817–1825. https://doi.org/10.1101/gr.197301.
19. "zein AND reviewed:yes in UniProtKB." https://www.uniprot.org/uniprot/?query=zein&fil=reviewed%3Ayes&sort=score (accessedSeptember 28, 2025).
20. "alpha zein AND reviewed:yes in UniProtKB." https://www.uniprot.org/uniprot/?query=alpha%20zein&fil=reviewed%3Ayes&sort =score (accessed September 28, 2025).
21. Wang, Y.; Padua, G.W. Formation of Zein microphases in ethanol−water. *Langmuir* **2010**, *26*, 12897–12901. https://doi.org/10.1021/la101688v.
22. Forato, L.A.; Bicudo, T. D. C.; Colnago, L. A. Conformation of alpha Zeins in solid state by Fourier Transform IR. *Biopolymers* **2003**, *72*, 421–426. https://doi.org/10.1002/bip.10481.105
23. Tatham, A. S.; Field, J.M; Morris, V.J.; l'Anson, K.J.; Cardle, L.; Dufton, M.J.; Shewry, P.R. Solution conformational analysis of the alpha-Zein proteins of maize. *J. Biol. Chem.* **1993**, *268*, 26253–26259. https://doi.org/10.1016/S0021-9258(19)74308-7.
24. Forato, L.A.; Doriguetto, A. C.; Fischer, H.; Mascarenhas, Y. P.; Craievich, A. F.; Colnago,L. A. Conformation of the Z19 Prolamin by FTIR, NMR, and SAXS. *J. Agric. Food Chem.* **2004**, *52*, 2382–2385. https://doi.org/10.1021/jf035020+.
25. Argos, P.; Pedersen, K.; Marks, M.D.; Larkins, B.A. A Structural model for maize Zein proteins. *J. Biol. Chem.* **1982**, *257*, 9984–9990. https://doi.org/10.1016/S0021-9258(18)33974-7.
26. Matsushima, N.; Danno, G.; Takezawa, H.; Izumi, Y. Three-dimensional structure of maize alpha-Zein proteins studied by small-angle X-ray scattering. *Biochim. Biophys. Acta*. **1997**, *1339*, 14–22. https://doi.org/10.1016/s0167- 4838(96)00212-9.
27. Momany, F.A.; Sessa, D.J.; Lawton, J.W.; Selling, G.W.; Hamaker, S.A.H. Willett, J.L. Structural characterization of alpha-Zein. *J. Agric. Food Chem.* **2006**, *54*, 543–547. https://doi.org/10.1021/jf058135h.
28. Wang, Y.; Padua, G.W. Nanoscale characterization of Zein self-assembly. *Langmuir* **2012**, *28*, 2429–2435. https://doi.org/10.1021/la204204j.
29. Cui, X.; Wang, B.; Zhong, S.; Li, Z.; Han, Y.; Wang, H.; Moeewald, H. Preparation of protein microcapsules with narrow size distribution by sonochemical method. *Colloid Polym Sci* **2013**, *291*, 2271–2278. https://doi.org/10.1007/s00396-013-2962-5
30. Wang, Y.; Su, C.-P.; Schulmerich, M.; Padua, G. W. Characterization of core–shell structures formed by Zein, *Food Hydrocoll.* **2013**, *30*, 487– 494. https://doi.org/10.1016/j.foodhyd.2012.07.019.
31. Liu, Y.; Liang, Q.; Liu, X.; Raza, H.; Ma, H.; Ren, X. Treatment with ultrasound improves the encapsulation efficiency of resveratrol in Zein-gum arabic complex coacervates. *LWT – Food Science and Technology* **2022**, *153*, 112331. https://doi.org/10.1016/j.lwt.2021.112331

32. Feng Xue, Chen Li, Yanlong Liu, Xiangwei Zhu, Siyi Pan, Lufeng Wang, Encapsulation of tomato oleoresin with zein prepared from corn gluten meal, *Journal of Food Engineering*, **2013**, *119*, 439-445. https://doi.org/10.1016/j.jfoodeng.2013.06.012.
33. Ren, X,; Hou, T.; Liang, Q.; Zhang, X.; Hu, D.; Xu, B.; Chen, X.; Chalamaiah, M.; Ma, H. Effects of frequency ultrasound on the properties of zein-chitosan complex coacervation for resveratrol encapsulation. *Food Chemistry* **2019**, 279, 223-230. https://doi.org/10.1016/j.foodchem.2018.11.025.
34. Li, Y.; Xu, G.; Li, W.; Lv, L.; Zhang, Q. The role of ultrasound in the preparation of Zein nanoparticles/flaxseed gum complexes for the stabilization of Pickering emulsion. *Foods* **2021**, *10*, 1990. https://doi.org/10.3390/foods10091990
35. Padua, G.W.; Guardiola, L.V. Microcapsules produced from Zein, in Microencapsulation and Microspheres for Food Applications, Elsevier, **2015**, pp. 3– 20. https://doi.org/10.1016/B978-0-12-800350-3.00002-9.
36. Wu, Y.; Luo, Y.; Wang, Q. Antioxidant and antimicrobial properties of essential oils encapsulated in Zein nanoparticles prepared by liquid–liquid dispersion method. *LWT - Food Sci. Technol.* **2012**, *48*, 283–290. https://doi.org/10.1016/j.lwt.2012.03.027.
37. Rasteh, I.; Pirnia, M.; Amin Miri, M.; Sarani, S. Encapsulation of Zataria multiflora essential oil in electrosprayed Zein microcapsules: Characterization and antimicrobial properties, *Industrial Crops and Products* **2024**, *208*, 117794. https://doi.org/10.1016/j.indcrop.2023.117794.
38. Zhong, Q.; Jin, M.; Davidson, P.M.; Zivanovic,S. Sustained release of lysozyme from Zein microcapsules produced by a supercritical anti-solvent process. *Food Chemistry* **2009**, *115*, 697-700. https://doi.org/10.1016/j.foodchem.2008.12.063.
39. Klymchenko, A.S. Fluorescent probes for lipid membranes: From the cell surface to organelles. *Acc. Chem. Res.* **2023**, *56*, 1-12. https://doi.org/10.1021/acs.accounts.2c00586
40. Feng, Y.; Liu, W.; Mercadé-Prieto, R.; Chen X. D. Dye-protein interactions between Rhodamine B and Whey proteins that affect the photoproperties of the dye. *J. Photochem. Photobiol. Chem.* **2021**, *408*, 113092. https://doi.org/10.1016/j.jphotochem.2020.113092.
41. Stokes, D.J.; Thiel, B.L.; Donald, A.M. Direct observation of water−oil emulsion systems in the liquid state by Environmental Scanning Electron Microscopy. *Langmuir* **1998**, *14*, 4402–4408. https://doi.org/10.1021/la980281c.
42. Kirk, S.E.; Skepper, J.N.; Donald, A.M. Application of Environmental Scanning Electron Microscopy to determine biological surface structure. *J. Microsc*. **2009**, *233*, 205–224. https://doi.org/10.1111/j.1365-2818.2009.03111.x.
43. Beaven, G.H.; Holiday, E.R. Ultraviolet absorption spectra of proteins and amino acids, *Advances in Protein Chemistry*, 1952, pp. 319– 386. https://doi.org/10.1016/S0065-3233(08)60022-4.
44. Malencik, D.A.; Anderson, S.R. Dityrosine as a product of oxidative stress and fluorescent probe. *Amino Acids* **2003**, *25*, 233–247. https://doi.org/10.1007/s00726-003-0014-z
45. Heinecke, J.W.; Li, W.; Daehnke, H.L.; Goldstein, J. A. Dityrosine, a specific marker of oxidation, is synthesized by the Myeloperoxidase-Hydrogen Peroxide system of human neutrophils and macrophages. *J. Biol. Chem.* **1993**, *268*, 4069–4077. https://doi.org/10.1016/S0021-9258(18)53581-X
46. Nguyen, D.D.; Johnson, S.K.; Clarke, M.W. Identification and quantification of dityrosine in grain proteins by isotope dilution liquid chromatography-tandem mass spectrometry. *Food Anal. Methods*, **2017**, *10*, 3321–3328. https://doi.org/10.1007/s12161-017-0901-7.
47. BeStSel: a web server for accurate protein secondary structure prediction and fold recognition from the circulardichroism spectra. Nucleic Acids Research, Oxford Academic. https://academic.oup.com/nar/article/46/W1/W315/5035652?login=false.
48. Zhao, H.; Fei, X.; Cao, L.; Zhao, S.; Zhou, J. Changes in microcapsules under heating: the effect of particle size on thermal stability and breakability. *J. Mater. Sci.* **2020**, *55*, 3902–3911. https://doi.org/10.1007/s10853-019-04297-8.
49. Hewlings, S.J.; Kalman, D.S. Curcumin: A review of its' effects on human health, *Foods* **2017**, *10*, 92. https://doi.org/10.3390/foods6100092.

50. Kharat, M.; Du, Z.; Zhang, G.; McClements, D.J. Physical and chemical stability of Curcumin in aqueous solutions and emulsions: Impact of pH, temperature, and molecular environment. *J. Agric. Food Chem.* **2017**, *65*, 1525−1532. https://doi.org/10.1021/acs.jafc.6b04815
51. C. F. Chignell, C.F.; Bilski, P.; Reszka, K.J.; Motten, A. G.; Sik, R. H.; Dahl, T. A. Spectral and photochemical properties of Curcumin. *Photochem. Photobiol.* **1994**, *59*, 295–302. https://doi.org/10.1111/j.1751-1097.1994.tb05037.x
52. Hu, K.; Huang, X.; Gao, Y.; Huang, X.; Xiao, H.; McClements, D.J. Core-shell biopolymer nanoparticle delivery systems: Synthesis and characterization of Curcumin fortified Zein-Pectin nanoparticles. *Food Chem.* **2015**, *182*, 275-281. https://doi.org/10.1016/j.foodchem.2015.03.009
53. Dai, L.; Sun, C.; Li, R.; Mao, L.; Liu, F.; Gao, Y. Structural characterization, formation mechanism and stability of Curcumin, in Zein-Lecithin composite nanoparticles fabricated by antisolvent co-precipitation. *Food Chem.* **2017**, *237*, 1163-1171. https://doi.org/10.1016/j.foodchem..2017..05.134
54. Chen, S.; Han, Y.H.; Huang, J.Y.; Dai, L.; Du, J., McClements, D.J.; Mao, L.; Liu, J.; Gao, Y.X. Fabrication and characterization of layer-by-layer composite nanoparticles based on Zein and Hyaluronic acid for co-delivery of Curcumin and Quercetagetin, *ACS Appl. Mater. Interf.* **2019**, *11*, 16922-16933. https://doi.org/10.1021/acsami.9b02529
55. Liu, Q.; Jing, Y.; Han, C.; Zhang, H.; Tian, Y. Encapsulation of Curcumin in Zein/Caseinate/sodium Alginate nanoparticles with improved physico-chemical and controlled release properties. *Food Hydrocoll.* **2019**, *93*, 432-442. https://doi.org/10.1016/j.foodhyd.2019.02-003
56. Feng, S.; Sun, Y.; Wang, D.; Sun, P.; Shao, P. Effect of adjusting pH and Chondroitin sulfate in the formation of Curcumin Zein nanoparticles: Synthesis, characterization and morphology. *Carbohydr. Polym.* **2020**, *250*, 116970. https://doi.org/10.1016/j.carbpol.2020.116970
57. Chen, S.; Li, Q.; McClements, D.J.; Han, Y.H.; Dai, L.; Mao, L.; Gao, Y.X. Co-delivery of Curcumin and Piperine in Zein-Carrageenan core-shell nanoparticles: Formation, structure, stability and in vitro gastrointestinal digestion. *Food Hydrocoll.* **2020**, *99*, 105334. https://doi.org/10.1016/j.foodhyd.2019.105334
58. Liu, J.; Li, Y.; Zhang, H.; Liu, S.; Yang, M.; Cui, M.; Zhang, T.; Yu, Y.; Xiao, H.; Du, Z. Fabrication, characterization and functional attributes of Zein-Egg White derived peptides (EWDP)-chitosan tertiary nanoparticles for encapsulation of Curcumin: Role of EWDP. *Food Chem.* **2022**, *372*, 131266. https://doi.org/10.1016/j.foodchem.20121.131266
59. Peng, Y.; Li, X.; Gu, P.; Cheng, W.; Zhang, R.; Hu, K. Curcumin-loaded Zein/Pectin nanoparticles: Caco-2 cellular uptake and the effects on cell cycle arrest and apoptosis of human hepatoma cells (HepG2). *J. Drug Deliv. Sci. Technol.* **2022**, *74*, 103497. https://doi.org/10.1016/j.jddst.2022.103497
60. Zhang H.; Shi, X.; Li, Y,; Li, S.; Zhang, L.; Huang, X.; Yang, M.; Du, Z.; Liu, J.; Zhang, T. Enhancing the stability and biological activity of Curcumin through incorporating Zein-sodium Alginate-egg white peptides hybrid assemblies. *Food Bioscience* **2024**, *59*, 103868. https://doi.org/10.1016/j.fbio.2024.103868.
61. Yang, J.; Chen, X.; Lin, J.; Shen, M.; Wang, Y.; Sarkar, A.; Wen, H.; Xie, J. Co-delivery of Resveratrol and Curcumin based on Mesona chinensis polysaccharides/Zein nanoparticle for targeted alleviation of ulcerative colitis. *Food Bioscience* **2024**, *59*, 104060. https://doi.org/10.1016/j.fbio.2024.104060.
62. Mondal, S.; Ghosh, S.; Moulik, S. P. Stability of Curcumin in different solvent and solution media: UV–Visible and steady-state fluorescence spectral study. *J. Photochem. Photobiol. B* **2016**, *158*, 212–218. https://doi.org/10.1016/j.jphotobiol.2016.03.004.
63. Lakowicz, J.R. Principles of Fluorescence Spectroscopy, 3rd ed. New York: Springer, 2006.
64. Abràmoff, M.D.; Magalhães, P.J.; Ram, S.J. Image Processing with ImageJ. *Biophotonics Int.*, **2004**, *11*, 36–42.
65. Danilatos, G. D. Foundations of Environmental Scanning Electron Microscopy, in *Advances in Electronics and Electron Physics*, P. W. Hawkes, Ed. Academic Press, **1988**, *71*, 109-250. https://doi.org/10.1016/S0065-2539(08)60902-6.
66. Pan, Y.; Tikekar, R.V.; Wang, M.S.; Avena-Bustillos, R.J.; Nitin, N. Effect of barrier properties of Zein colloidal particles and oil-in-water emulsions on oxidative stability of encapsulated bioactive compounds. *Food Hydrocoll.* **2015**, *43*, 82–90. https://doi.org/10.1016/j.foodhyd.2014.05.002.
67. Pulido-Moran, M.; Moreno-Fernandez, J.; Ramirez-Tortosa, C.; Ramirez-Tortosa, M. C. Curcumin and health. *Molecules* **2016**, *21*, 52-57. https://doi.org/10.3390/molecules21030264

 doi:10.20944/preprints202510.0678.v1

68. Anand, P.; Kunnumakkara, A. B.; Newman, R. A.; Aggarwal, B. B. Bioavailability of Curcumin: Problems and promises. *Molecular Pharmaceutics* **2007**, *4*, 807–818. https://doi.org/10.1021/mp700113r: